**SO STRESSED OUT! CHARACTERIZING THE STRESS STATE NEAR ENCELADUS' IMPACT CRATERS USING 3D FINITE ELEMENT MODELING.** Mallory J. Kinczyk[1], Paul K. Byrne[2], Kathleen L. Craft[1]. [1]The Johns Hopkins University Applied Physics Laboratory, Laurel, MD 20723, [2]Department of Earth and Planetary Sciences and McDonnell Center for the Space Sciences, Washington University, Saint Louis, MO, 63130.

**Introduction:** Among the many unique features of Saturn's icy moon Enceladus are a variety of geological landforms that suggest temporal and spatial variations in the state of stress of the shell on a global scale [e.g., 1-4]. The cratered terrains of Enceladus comprise ~40% of the surface and have received little attention from researchers due to the perceived lack of geological activity there. Notable in the cratered terrains, however, are systems of narrow fractures that crosscut many of the craters in this region (**Fig. 1**). In some instances, these fractures have orientations that change in proximity to, and so appear influenced by, craters. The fractures appear to be extensional in nature and, based on their morphology, are likely expressions of some of the most recent tectonic activity at Enceladus [5].

The apparent phenomenon of fracture reorientation is of interest because Enceladus is the only cratered body in the Solar System where, so far, many instances of such interaction have been identified, unlike other geologically active icy moons such as Europa and Triton [6]. We hypothesize that the apparent change of fracture orientation with proximity to craters on Enceladus results from a combination of small effective elastic thickness ($T_e$) relative to the diameter of impact craters present and regional-scale flexure of the ice shell. Here, we present preliminary results from three-dimensional structural numerical modeling to gain insight into the relative influence of crater size and $T_e$ on fracture reorientation in Enceladus' cratered terrain.

**Methods:** A 3D finite-element engineering software, ANSYS, was used to model a single crater in a homogeneous elastic plate with a thickness corresponding to the estimated $T_e$ of Enceladus' icy shell [7,8]. We simulate two loading scenarios (**Fig. 2**)—uniaxial horizontal extension and flexure via upward loading—and determine the orientation of principal stresses relative to the modeled crater.

These two model scenarios are based on geological processes that have been proposed to be occurring at Enceladus and that parallel geological processes on Earth. Our model of uniaxial extension follows examples of horizontal extension and contraction that have been modeled for the trailing hemisphere terrain of Enceladus [9], where unstable extension and lithospheric necking were proposed to have occurred in a brittle layer overlying a viscous substrate arising from intense localized heating. Our flexural model is based on proposed convection theories in the ice shell [10] or isostatic adjustment [11] of an uncompensated shell.

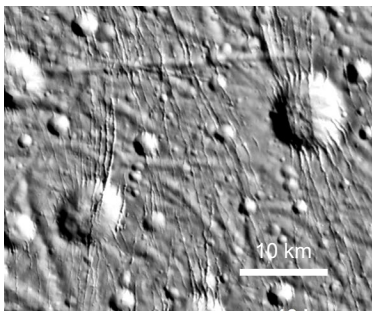


**Figure 1.** Cratered terrain (5°N, 165°E). The fracture network trending N–S shows both straight and deflected segments proximal to the two large craters.

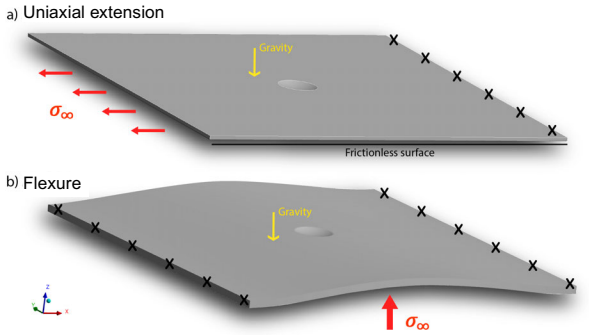


**Figure 2.** Model boundary conditions for two scenarios for a single crater in an elastic plate. (a) Uniaxial extension with an applied, distributed tensile stress. (b) Flexure via upward loading is applied directly beneath the crater.

The crater's size is fixed at 10 km in diameter with a depth–diameter ($d/D$) ratio of 0.1, which is the approximate ratio for simple craters on icy satellites [12]. The elastic plate dimensions were 100 × 100 km, and the thickness of the plate was varied between $T_e$ = 500 m, 1 km, and 2 km. We assumed that the brittle icy shell of Enceladus was homogeneous, isotropic polycrystalline water ice I, with the properties as defined in **Table 1** and published in the literature [7, 13–16]. The models were composed of a tetrahedral mesh with a 600 m element size within 12 km of the crater center and a 2 km element size beyond that.

**Table 1.** Model parameters for polycrystalline water Ice I.

| Property | Value |
|---|---|
| Young's Modulus (E) | $8.87\times10^9$ Pa |
| Poisson's Ratio (v) | 0.344 |
| Bulk Modulus (K) | $9.5\times10^9$ Pa |
| Shear Modulus (S) | $3.3\times10^9$ Pa |
| Compressive Yield Strength ($\sigma_{3\ crit}$) | $5.2\times10^7$ Pa |
| Tensile Yield Strength ($\sigma_{1\ crit}$) | $1.5\times10^6$ Pa |
| Density ($\rho$) | 925 kg/m$^3$ |
| Gravitational Acceleration (g) | 0.113 m/s$^2$ |
| Applied remote stress ($\sigma_\infty$) | Model A: $1.3\times10^6$ Pa<br>Model B: $3\times10^5$ Pa |

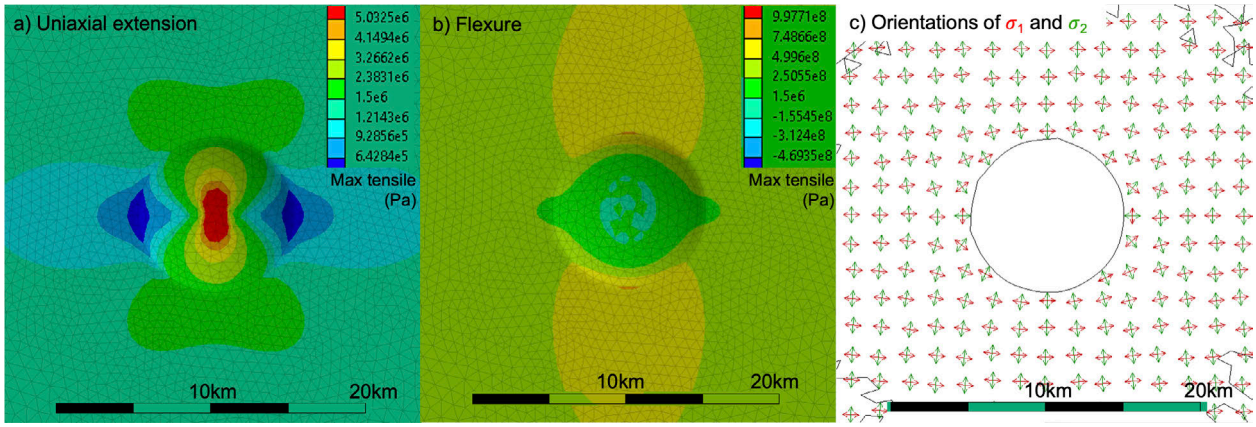


**Figure 3.** Magnitudes of maximum tensile stress ($\sigma_1$) within a 1000 m-thick elastic plate for (a) uniaxial extension and (b) upward-directed flexure. The crater acts as a stress concentration, with $\sigma_1$ elevated at the northern and southern edges of the crater rim and a stress shadow forming perpendicular to the direction of $\sigma_1$. (c) Orientations of $\sigma_1$ and $\sigma_2$ in red and green respectively.

The applied load was determined based on the minimum load requirement for potential failure at the crater rim (i.e., exceeding the maximum tensile strength of ice of 1.5 MPa) in the model with the largest value of $T_e$. Under uniaxial horizontal extension, the necessary load was 1.3 MPa, approximately four times greater than that required for failure in the flexural model (0.3 MPa). For reference, the magnitude of diurnal tidal stresses at Enceladus is ~0.1 MPa [e.g., 17]. **Fig. 3** shows an intermediate model with $T_e$ set at 1000 m. We then evaluated the orientations of principal stresses at each node (**Fig. 3c**), where $\sigma_1$ is maximum tensile stress and $\sigma_3$ is the maximum compressive stress. Since, in most cases, $\sigma_3$ is oriented vertically, model results focus on $\sigma_2$ as an indication of the horizontal direction of fracture propagation, since fractures propagate along-strike parallel to $\sigma_2$. Because the data here are axial (i.e., bi-directional), we converted $\sigma_2$ orientations from axial directions (0–360°) to unimodal vectors oriented ±90° from the geographical north and computed the circular variance of orientations (i.e., dispersion) [18] where low dispersion values indicate more uniform $\sigma_2$ orientations and high values indicate a greater spread of orientations.

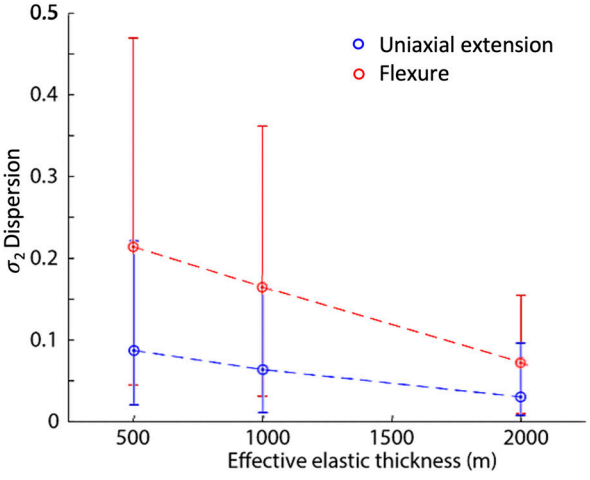


**Figure 4.** Dispersion, of $\sigma_2$ orientations at the crater rim, as a function of $T_e$. Less dispersion is observed for uniaxial extension compared with flexure across all plate thicknesses.

**Results: Fig. 4** displays the calculated dispersion of orientations of $\sigma_2$ at the crater rim from both uniaxial extension and flexure across the range of $T_e$ considered here. We find that the calculated dispersion is greater for flexure across all plate thicknesses than for all scenarios of uniaxial extension. The dispersion of $\sigma_2$ orientations also decreases with increasing plate thickness. We take the orientation of $\sigma_2$ at the mesh nodes located at the crater rim as representative of fracture orientation and therefore suggest that fracture reorientation is more likely to occur in a region of the ice shell experiencing flexure and less likely in regions experiencing uniaxial extension. We further infer that strike reorientation is more likely to occur in a shell with lower values of $T_e$. Future work will compare the orientations of modeled principal stresses with the strikes of mapped fractures on Enceladus to establish the stress state that most closely fits our observations. By doing so, we will take a useful step in understanding the stress mechanisms that have or are currently deforming Enceladus' cratered terrain.

**References:** [1] Patterson, et al. (2018), *Enc. & the Icy Moons of Sat.* (pp. 95–125). [2] Bland, et al. (2012), GRL, 39(17),1-5. [3] Kinczyk, et al. (2022), LPS, 54, 1144. [4] Martin, et al. (2016) GRL, 43, 2456-2464. [5] Martin et al. (2017) Icarus, 294, 209–217. [6] Martin, et al. (2011) LPS, 42, 2666. [7] Čadek, et al. (2016), GRL, 43(11), 5653–5560. [8] Giese, et al. (2008) GRL, 35(24), 1–5. [9] Bland, et al. (2007), Icarus, 192(1), 92–105. [10] Barr & McKinnon (2007) GRL, 34(9), 2–7. [11] Hemingway, et al. (2018), Enceladus & Icy Moons of Sat., pp. 57–77. [12] Schenk (1989) JGR, 94(B4), 3813–3832. [13] Beuthe (2015) Icarus, 248, 109–134. [14] Schulson, et al. (2006) Met. Plan. Sci., 41(10), 1497–1508. [15] Petrovic (2003) JMS, 8,1–6. [16] Litwin, et al. (2012) JGRP, 117(8), 1–14. [17] Hurford, et al. (2007) Nature, 447(7142), 292–294. [18] Berens (2009) Journ. Stat. Soft. 31(10), 1–21.